Journal of Advanced Ceramics
2018, **7**(2): 89–98
https://doi.org/10.1007/s40145-018-0260-x
ISSN 2226-4108
CN 10-1154/TQ

Research Article

Optimal design on the high-temperature mechanical properties of porous alumina ceramics based on fractal dimension analysis

Jingjing LIU[a,b], Wenlong HUO[a], Xiaoyan ZHANG[a], Bo REN[a,*], Yuanbing LI[b], Zaijuan ZHANG[a], Jinlong YANG[a,*]

[a]*State Key Laboratory of New Ceramics and Fine Processing, School of Materials Science and Engineering, Tsinghua University, Beijing 100084, China*
[b]*State Key Laboratory of Refractories and Metallurgy, Wuhan University of Science and Technology, Wuhan 430081, China*

Received: November 13, 2017; Revised: January 20, 2018; Accepted: January 21, 2018

Abstract: Fractal theory and regression analysis were employed for the first time to investigate the effect of pore size and pore distribution on high-temperature mechanical properties of porous alumina ceramics (PAC). In the present work, PAC with the comparable porosity, different pore sizes and pore distributions were prepared using carbon black as the pore-forming agent. Particular emphasis in this study was placed on the establishment of correlation between the thermal shock resistance and pore properties. The relationship between fractal dimension (D_f) and thermal shock resistance parameter (R_{st}) in specimens presented the negative power function, indicating that low D_f could benefit the improvement of thermal shock resistance in specimens. The results showed that the increase of pore size and pore sphericity leads to a reduced D_f, the enhanced hot modulus of rupture (HMOR) and R_{st}. The decrease of proportion of micro-pores below 2 μm, the increase of mean pore size and pore sphericity could result in the decrease of D_f, and then improve R_{st} and HMOR of specimens. Based on the correlation between R_{st} and pore characteristics, PAC with improved thermal shock resistance could be achieved when their pore structure meets the above features.

Keywords: porous alumina ceramics (PAC); pore size; thermal shock resistance; high-temperature mechanical properties; fractal dimension

1 Introduction

Porous alumina ceramics (PAC) have attracted considerable attention as thermal insulators, gas/liquid filters, catalytic supports, and high-temperature structural material, due to their high-temperature refractoriness, high surface area, and low thermal conductivity [1–3]. In the majority of applications, PAC often encounter strong heat flow and/or abrupt temperature shock, leading to instantaneous thermal stresses. Consequently, a large amount of cracks initiate and then propagate rapidly, resulting in the thermal shock damage. In fact, the fabrication of PAC with excellent thermal mechanical properties of the porous ceramics depends not only on the chemical design but also on the pore structure design of the specimens.

It was found that mullite and spinel exhibit great benefits on enhancement of thermal shock resistance

* Corresponding authors.
E-mail: B. Ren, rb881228@126.com;
J. Yang, jlyang@mail.tsinghua.edu.cn

because of the thermal expansion coefficient mismatch of two phases [4–7]. As for the porosity, Shyam *et al.* [8] found high porosity shows great benefits on enhancement of thermal shock resistance of porous ceramics since both crack propagation and thermal stress in ceramics are generally absorbed by porosity. It was reported by Jin *et al.* [9] that the increase of porosity and decrease of pore size also result in superior thermal shock resistance. Besides these results, further investigations explored by She *et al.* [10] confirm that increase of porosity also deteriorates thermal shock damage resistance due to the crack initiation caused by more pores. The conclusions about porosity dependence of thermal shock fracture resistance could be explained by Hasselman's unified theory.

Recently, some researchers revealed that the thermal shock resistance of porous ceramics could also be modified and optimized by some other pore-related characteristics (i.e., pore morphology, proportion of micro-pores, and pore size distribution) [11,12]. Pore-related characteristics, such as pore size and morphology on the effect of thermal shock resistance of ceramic materials have been reported [13–15]. For example, Lee *et al.* [13] used finite element simulations to investigate the influence of pore morphology on thermal shock resistance of porous ceramics and found that their thermal shock resistance is enhanced obviously when the pore shape changes from spherical to ellipsoidal. Jin *et al.* [14] found the critical difference temperature (ΔT_c) of porous Al_2O_3–ZrO_2 ceramics shows a deceasing trend with increasing the pore size from 2.21 to 4.23 μm. However, all these interesting results were failed to describe the relationship between pore-related characteristics and their thermal shock resistance quantitatively, which was attributed to the difficulty in characterization of such pore-related parameters.

Fractal theory, introduced firstly by Mandelbrot, has become an important tool to describe the feature of irregular pores quantitatively in ceramic materials [16–18]. It builds a bridge between micro and macroscale properties and makes the description of macro-performance with micro-morphology possible from qualitative to quantitative. In the past decades, this approach has been extensively used to analyze the correlation between the pore-related characteristics and the performance (including thermal conductivity, strength, and elastic modulus, etc.), aiming to fabricate porous ceramics with excellent thermal insulation and mechanical performance [19–22]. So far, a majority of the studies about the fractal analysis have focused on the effect of pore structure on mechanical strength and thermal conductivity of porous ceramics. Nerveless, a clear understanding of the pore structure effect on thermal shock resistance of porous ceramics is lacking.

To the best of our knowledge, there is no quantitative relationship to predict the thermal shock resistance of PAC with fractal pore size and pore distribution. In this study, PAC with different pore size and pore distribution are fabricated to investigate the effect of the above pore-related characteristics on their thermal mechanical properties. Particular investigation emphasis is placed on the thermal shock resistance. To achieve this goal, fractal dimension and regression analysis are employed for the first time to further understand the dependence of pore structure on thermal shock resistance. Based on the above results, PAC with improved thermal shock resistance are obtained. This work makes a contribution to the effect of pore characteristics on performance of PAC.

2 Experiment

2.1 Materials and preparation

In this study, tabular alumina (⩽ 74 μm and ⩽ 45 μm, Qingdao Almatis Premium Alumina Co., Ltd., China), α-Al_2O_3 (2 μm, Kaifeng Special Refractories Co., Ltd., China), ρ-Al_2O_3 (5 μm, Kaifeng Special Refractories Co., Ltd., China), and metallic Al powder (⩽ 45 μm, Xinxiang Zhongyuan Alumina Material Co., Ltd., China) were used as the main raw materials. Four different types of carbon black (CB, N220, 20–30 nm; N330, 30–50 nm; N774, 40–100 nm; N990, 100–700 nm, Wuhan Kebang New Material Co., Ltd., China) and commercially available polyvinyl alcohol solution (PVA, liquid with solid content of 8 wt%) were used as pore-forming agents and binder, respectively. It is worth noting that the incorporation amount of carbon black for all the specimens was the same to ensure that the apparent porosities of all fired specimens were kept in the same level. On the other hand, different types of carbon black were introduced to adjust the pore size and pore distribution of specimens. Therefore, the role of other pore-related characteristics except porosity could be investigated. In this work, the addition amount of carbon black was 25 wt% for each specimen. The batch compositions are presented in Table 1. The

mixture of raw materials was firstly wet-milled with a rotating speed of 300 rpm for 3 h in a planetary balling (corundum balls as the abrasive media) using absolute ethyl alcohol as dispersion medium. The mass ratio of the raw materials to corundum balls and absolute ethyl alcohol was 1:3:1. The as-prepared mixtures were mixed with 8 wt% PVA solution in a mixer for 30 min with the rotating speed of 80–100 rpm after drying at 110 ℃ for 24 h. After kneading, the specimens with different dimensions were compacted under a pressure of 10 MPa by a hydraulic press, then cured at 110 ℃ for 24 h in a muffle furnace. Subsequently, the as-obtained specimens were sintered with a heating rate 5 ℃/min to 1600 ℃, and then kept at 1600 ℃ for 3 h in air using an electric furnace. The disc-shaped specimens (Φ180 mm × 20 mm) were fabricated to determine the thermal conductivity. The bar-shaped specimens (25 mm × 25 mm × 140 mm) were used for the three-point bending and modulus of elasticity tests and columnar specimens (Φ10 mm × 50 mm) for thermal expansion coefficient test. For each point, five samples were measured to obtain the mean and standard deviations of strength.

2. 2 Characterization

The apparent porosity and bulk density of the sintered specimens were measured according to the Archimedes' principle. The total porosity (V_p) of the sintered specimens was obtained from the bulk and true densities using the following equation:

$$V_p = 1 - \frac{\rho_{bulk}}{\rho_{true}} \quad (1)$$

where the true density (ρ_{true}) of alumina is 3.98 g/cm^3. The linear change ratio was calculated according to the expression $S = (L_0 - L_1)/L_0 \times 100\%$, where the lengths L_0 and L_1 before and after sintering in specimens were measured respectively. The microstructures of the specimens were observed using scanning electron microscopy (SEM; MERLIN VP Compact, Carl Zeiss, Jena, Germany). Pore structure parameters were analyzed based on the microstructure photographs using Micro-Images Analysis & Process System (MIAPS) software (Beijing Precise Instrument Co., Ltd., China), and the detailed calculation method is shown in Ref. [23]. Thermal conductivity of sintered specimens was measured via the standard water flow plate method (PBD-30, Sinosteel Luoyang Institute of Refractories Research Co., Ltd., China). Hot modulus of rupture (HMOR) of the sintered specimens at 200–1400 ℃ was also measured under a three-point mode using an electronic digital control system (HMOR-03AP, Luoyang Precondar Instruments for Testing Refractoriness Co., Ltd., China). The thermal expansion coefficient (α, room temperature to 1400 ℃) of the specimens after treating at 1400 ℃ was measured via a thermal dilatometer (Unitherm™ model 1161 dilatometer system, Anter Corp., Pittsburgh, PA, USA). Moreover, thermal shock behavior of the sintered specimens after treating at 200–1100 ℃ was characterized by air quenching method for 3 thermal shock cycles. The residual strength ratio of thermal shock was calculated according to the expression $M = S_0 / S_1 \times 100\%$, where the strengths of specimens before and after thermal shock cycle were S_0 and S_1, respectively. All the above properties measured for each composition were average values from three test pieces.

3 Results and discussion

3. 1 Microstructure of PAC

The apparent porosity (AP) and bulk density (BD) of the sintered specimens are shown in Table 2. As expected, there is no significant difference in the porosity of specimens, which is attributed to the incorporation of the same amount of pore-forming agent. Thus, any

Table 1 Batch compositions of the specimens

(Unit: wt%)

Ingredient	C220	C330	C774	C330-774	C330-990
Tabular alumina	20	20	20	20	20
α-Al_2O_3 powder	74	69	64	54	49
ρ-Al_2O_3	5	5	5	5	5
Carbon black (25 wt%)	N220	N330	N774	N330:N774 (1:1 in mass ratio)	N330:N990 (1:1 in mass ratio)
Metal Al	1	1	1	1	1
PVA	+8	+8	+8	+8	+8

Table 2 Physical properties of porous alumina specimens with different types of carbon black

Property	Carbon content 25 wt%, 1600 ℃				
	C220	C330	C774	C330-774	C330-990
BD (g/cm^3)	1.39	1.42	1.42	1.35	1.40
AP (%)	64.9	64.3	63.9	65.9	64.7
LCR (%)	–7.98	–4.54	–7.98	–7.28	–5.53
LCRR (%)	–3.63	–0.75	–0.86	–1.16	–1.24

differences on thermal mechanical properties can be attributed to other pore characteristics except porosity. On the other hand, the removal of carbon black and rearrangement of particles also contribute to the decrease of interparticle distance [24]. As a result, the linear change shrinkage (LCR) and linear shrinkage of reheating (LCRR) are observed for each specimen. For instance, the LCR value of specimen C330-774 is 7.28%, while its LCRR is 1.16%.

Microstructures of the polished surface of different PAC specimens are shown in Fig. 1, and their higher magnification morphologies are shown in the insets. As shown in Fig. 1(a), some amounts of spherical pores are distributed homogeneously in specimen C220. For specimens C330 and C774, although their porosities are controlled at the level of about 64%, their polished surface seems to be rough where more interconnected pores generate, which is probably due to the increased of pore size (Figs. 1(b) and 1(c)). At higher magnification, the pores originated from the space among grains of specimen C774 are more irregular compared to those of C220 and C330. Meanwhile, much more spherical pores generate in specimens C330-774 and C330-990, and there are larger pores in the partial region of specimen C330-774 than those of specimen C330-990 (Figs. 1(d) and 1(e)). From their higher magnification, more spherical pores are generated compared with other specimens.

3. 2 Pore structure of PAC

In order to investigate the difference of pore structure between these specimens, mean pore size (MPS) and proportion of different pore size intervals are illustrated, as presented in Fig. 2 and Table 3, respectively. Although all specimens possess narrowed pore size distribution, their MPS and pore proportions are obviously different (Table 3). Specimen C330-990 possesses the highest proportion of pores of < 2 μm, which is 7.14%, and specimen C220 possesses the lowest proportion of pores of < 2 μm, which is 4.65%. In addition, the MPS of specimens C220, C330, C774, C330-774, and C330-990 are 4.24, 4.66, 5.37, 6.21, and 5.75 μm, respectively. This variation in MPS and pore proportions but the comparable porosity, for C220, C330, C774, C330-774, and C330-990, offers the possibility of investigating the property–pore size and its performance

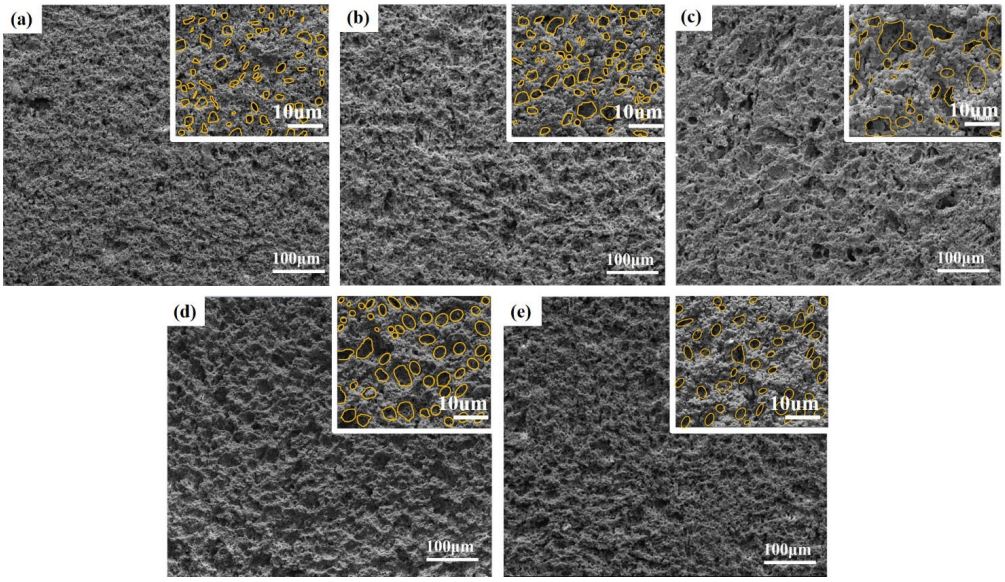

Fig. 1 SEM micrographs of specimens: (a) C220, (b) C330, (c) C774, (d) C330-774, and (e) C330-990.

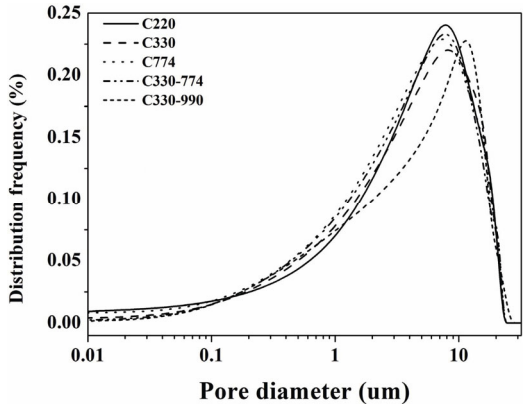

Fig. 2 Pore size distribution of porous alumina ceramics.

Table 3 Mean pore size, pore roundness, < 2 μm pore area, and > 18 μm pore area of the specimens

Specimen	< 2 μm pore area (%)	2–18 μm pore area (%)	> 18 μm pore area (%)	Mean pore size (μm)
C220	4.65	77.94	17.41	4.24
C330	6.19	77.42	16.39	4.66
C774	6.77	79.91	13.32	5.37
C330-774	6.87	80.79	11.34	6.21
C330-990	7.14	76.82	16.04	5.75

relationship.

In order to further reveal the pore structure changes in all specimens, the pore shape factor is calculated by the following equation:

$$R = \frac{P^2}{4\pi A} \tag{2}$$

where R represents the roundness of an individual pore, P and A denote the perimeter and area of an individual pore, respectively. Generally, a higher value for the pore shape factor always improves the irregularity of pores. In this case, the minimal value is 1 for a sphere according to Ref. [25] and the calculation results are shown in Fig. 3. The results show that specimen C774 possesses the highest R value among all specimens, which is 1.51 approximately, indicating the highest irregularity of pores. The result can be also verified in the microstructure observation. With increasing the particle size of pore-forming agent, lower R values are obtained for other specimens. Specimen C330-774 possesses the lowest pore shape factor, whose value is 1.39, which is also in good accordance with the previous microstructure shown in Fig. 1.

3. 3 Mechanical properties of PAC

The hot moduli of rupture (HMOR) of various specimens measured at 25–1400 ℃ are presented in Fig. 4. As can be seen, with increasing temperature,

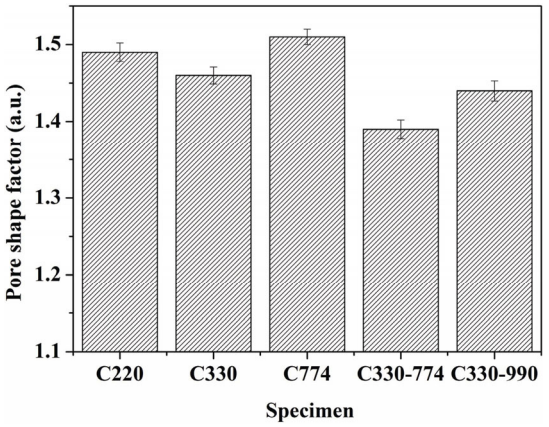

Fig. 3 Pore shape factor of porous alumina ceramics.

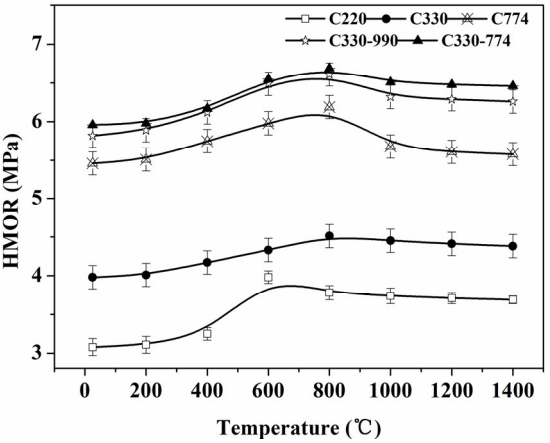

Fig. 4 Hot modulus of rupture of specimens with different types of carbon black.

HMOR of as-prepared specimens increases initially, then decreases, finally becomes quite stable. HMOR of each specimen reaches the maximum value upon increasing the testing temperature up to 600 or 800 ℃. Apparently, this behavior is different from conventional single-phase materials, but similar to that of composite materials [26], which can be attributed to the second phase. From Fig. 4, it also can be seen that at given temperatures, HMOR of specimen C330-774 is higher than that of specimen C220 despite they possess almost the same level of porosity. This phenomenon is inconsistent with the porosity–property prediction. This can be attributed to the larger difference in stress concentration in specimens caused by the different pore size and pore morphology. In addition, the sample C774 with the largest R shows the larger HMOR than that of specimen C220. This result can be attributed to the fact that highest proportion of > 18 μm pores and lowest proportion of < 2 μm result in smaller stress area per unit, thus leading to the decreasing of HMOR.

3. 4 Thermal shock resistance of PAC

Figure 5 shows the flexural strength and residual strength ratio of specimens as a function of quenching temperature. The residual strength ratio after thermal shock at 600 ℃ remains almost unchanged for all specimens. However, the residual strength ratios show an abrupt decrease for the specimens C220 and C330 with thermal shock treatment at temperature exceeding 600 ℃, and their residual strength ratios of 42.85% and 43.93% are observed at 1200 ℃, respectively. Meanwhile, the same occurrence is also detected over 800 ℃ and the higher residual strength ratios of 49.53%, 51.36%, and 53.18% are observed for specimens C774, C330-990, and C330-774 at 1200 ℃. Apparently, specimen C330-774 possesses the highest residual strength ratio among all of specimens, indicating the best thermal shock resistance.

This phenomenon can be explained by that the thermal shock resistance is not only affected by porosity, but also by pore size, proportion of micro-pores, and pore morphology of specimens.

To further characterize thermal shock resistance of PAC quantitatively, the thermal shock damage resistance parameters R', R'''', and R_{st} are introduced and then calculated by the following equations [27–29]:

$$R' = \Delta T_c = \frac{1-\mu}{E\alpha}\sigma_f \tag{3}$$

$$R'''' = \frac{1}{1-\mu}\left(\frac{K_{IC}}{\sigma_f}\right)^2 \tag{4}$$

$$R_{st} = \left(\frac{\gamma_f}{\alpha^2 E_0}\right)^{1/2} \tag{5}$$

where R', R'''', and R_{st} are the thermal shock damage resistance parameters of specimen, ΔT_c is the critical temperature difference, μ is the Poisson's ratio, E is the elasticity modulus, α is the linear coefficient of thermal expansion, σ_f is the fracture strength, K_{IC} is the fracture toughness, and γ_f is the fracture work. As shown in Table 4, R' and R'''' of specimens are 8.81–15.98 ℃ and 103.21–190.84, which are clearly inconsistent with the experimental results. Therefore, R' and R'''' are not capable to reflect their thermal shock resistance. With respect to R_{st}, specimens C330-774 and C220 exhibit the best and the worst thermal shock resistance, respectively, which fits well with experimental results. This occurrence can be explained by Hasselman's unified theory of thermal shock fracture initiation and crack propagation [30].

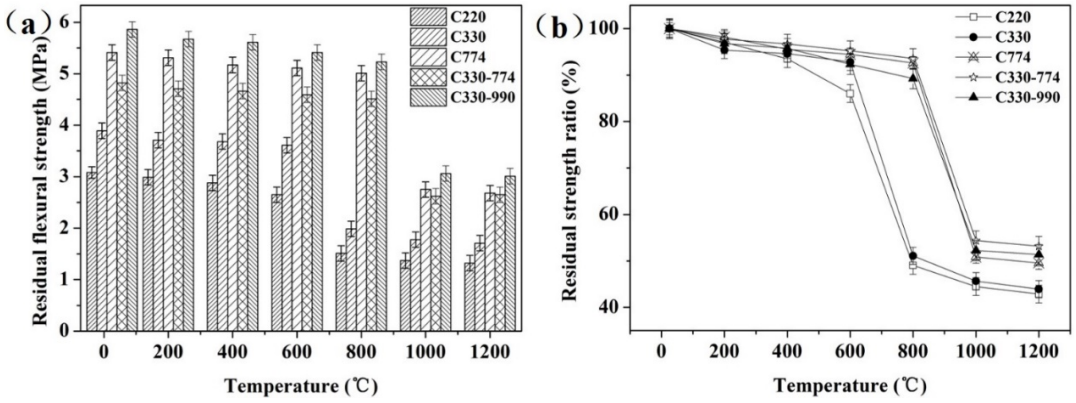

Fig. 5 Thermal shock resistance of porous alumina ceramics: (a) residual flexural strength and (b) residual strength ratio of specimens.

Table 4 Parameters of thermal shock resistance of PAC with different types of carbon black at critical temperature

	C220	C330	C774	C330-774	C330-990
σ_f (MPa)	1.82	2.56	3.15	3.89	4.13
Elastic modulus (GPa)	18.47	20.03	21.11	22.35	23.27
Thermal expansion α (10^{-6}/K)	8.11	8.07	8.38	8.11	8.05
K_{IC} (MPa·m$^{1/2}$)	22.26	40.55	43.32	64.70	65.01
γ_f (J·m^{-2})	13.41	41.06	44.45	93.67	90.80
R'	8.81	11.48	13.30	15.56	15.98
R''''	103.21	173.11	130.45	190.84	170.87
R_{st}	1.65	1.78	1.79	2.53	2.46

3. 5 Fractal analysis on pore structure of PAC

The above experimental results regarding mechanical properties and thermal shock resistance of PAC exhibit the same trend, and this occurrence can be explained by the variation of pore structure parameters (pore size, distribution, and shape factor) except porosity. In order to develop an accurate quantitative parameter for the pore size and its distribution, fractal dimension is employed to give a deeper understanding between pore size and its distribution and thermal shock resistance parameters (R_{st}) as well as mechanical strength. For this reason, the SEM photographs of all specimens in Fig. 1 are analyzed by extracting their pore boundaries with assistance of MIAPS and then the fractal dimension of all specimens is calculated. The results are shown in Fig. 6. The fractal dimension is calculated by slit island technique according to the equation [31]:

$$\log P = C + 0.5D_f \log A \quad (6)$$

where A and P refer to the area and perimeter of an individual pore respectively, C is a constant, and D_f is the fractal dimension whose value is normally in the range of 0–2. Generally, the higher the fractal dimension, the more complexity of pore structure. The calculation results of the fractal dimension are shown in Fig. 7. There is a good correlation between $\log A$ and $\log P$, especially when all the correlation coefficients are higher than 0.9, indicating that all the specimens have good fractal characteristics. As can be seen in Fig. 7, the specimen C220 possesses the maximum D_f value, which is 1.2214. With increasing the pore size, the D_f value becomes lower, and the lowest D_f value of 1.2042 is obtained for specimen C330-774. Afterwards, it rises again for specimen C330-990.

The relationships between D_f and thermal mechanical properties of specimens are also established, and the results are presented in Fig. 8. As can be seen in Fig. 8(a), R_{st} increases with the decrease of D_f. The relationship between R_{st} and D_f presents a power equation with a high correlation coefficient of 0.87. The exponent in regression equation is –53.25, which is negatively corrected, indicating higher D_f leads to the lower R_{st}. The regression results show that the relationship between HMOR and D_f also follows the power with a pretty high correlation coefficient of 0.75 (Fig. 8(b)). Based on the above analysis, it is possible to draw the conclusion that the improvement of mechanical property and thermo-mechanical property of the PAC can be obtained by decreasing D_f.

Since pore structures of PAC are constructed by fractal dimension, the relationships between pore characteristics and fractal dimension are also present in Fig. 9. The results show that D_f values of specimens

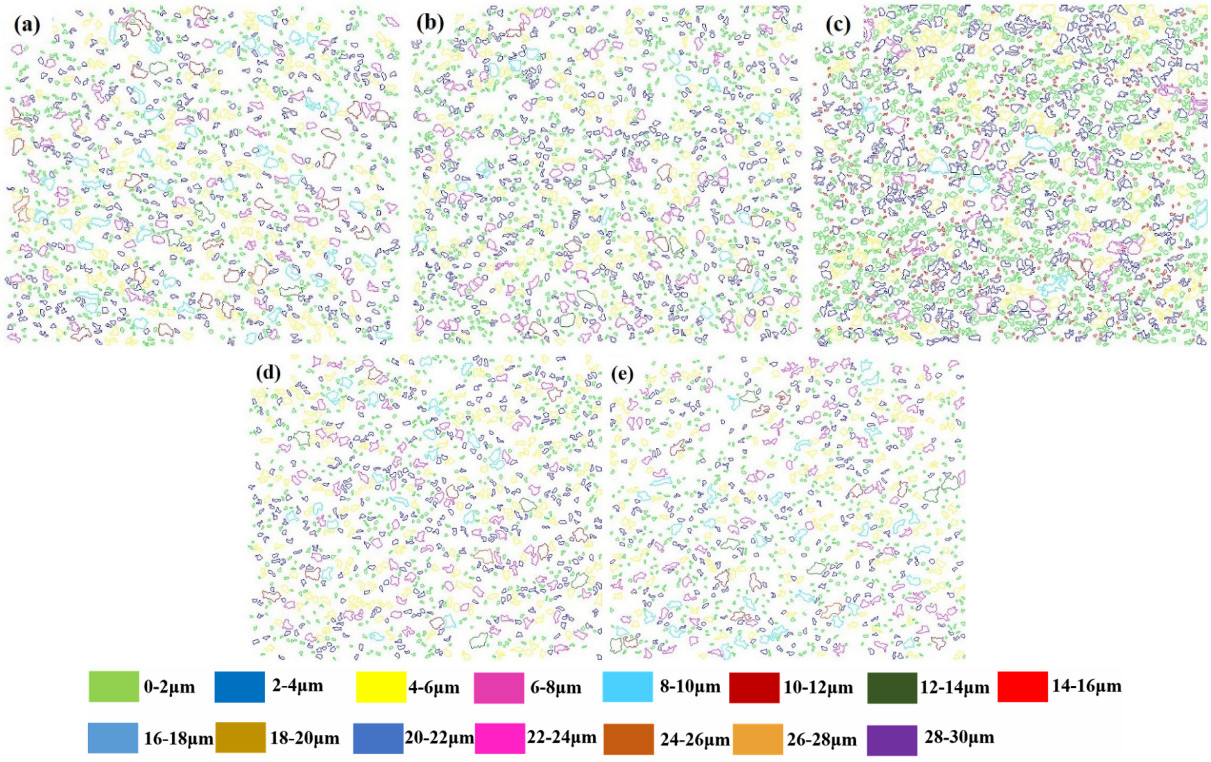

Fig. 6 Photographs of extracted pore boundary of specimens: (a) C220, (b) C330, (c) C774, (d) C330-774, and (e) C330-990.

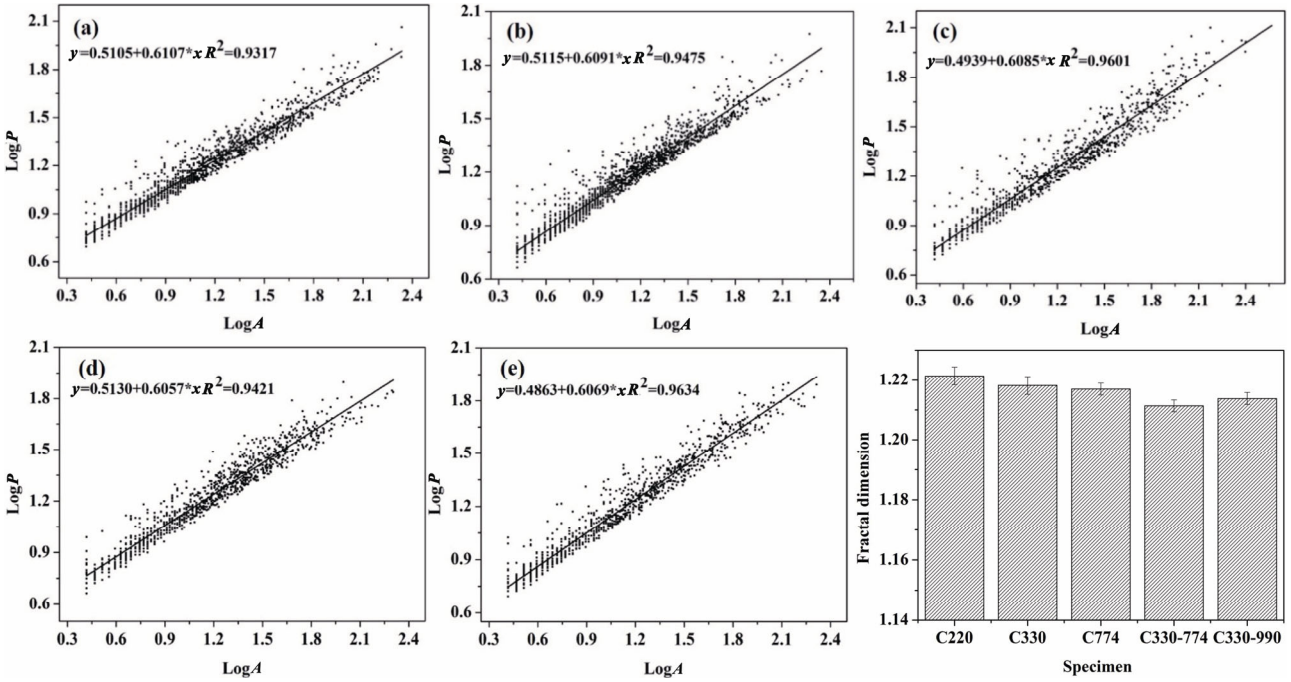

Fig. 7 Fractal dimension of specimens prepared with different types of carbon black.

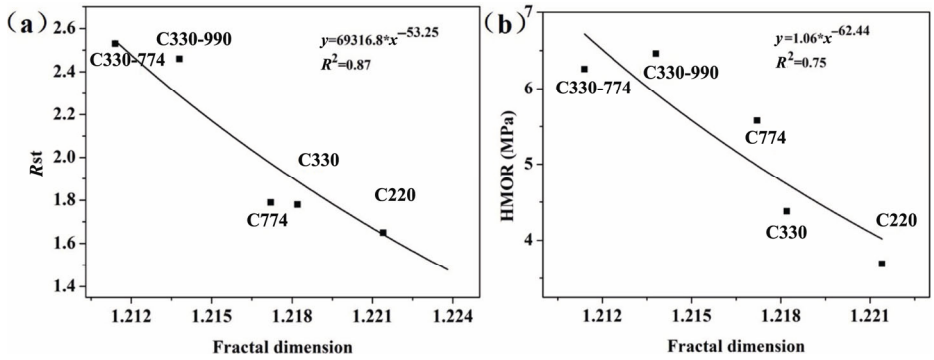

Fig. 8 Relationship between fractal dimension and (a) thermal shock resistance parameters and (b) HMOR.

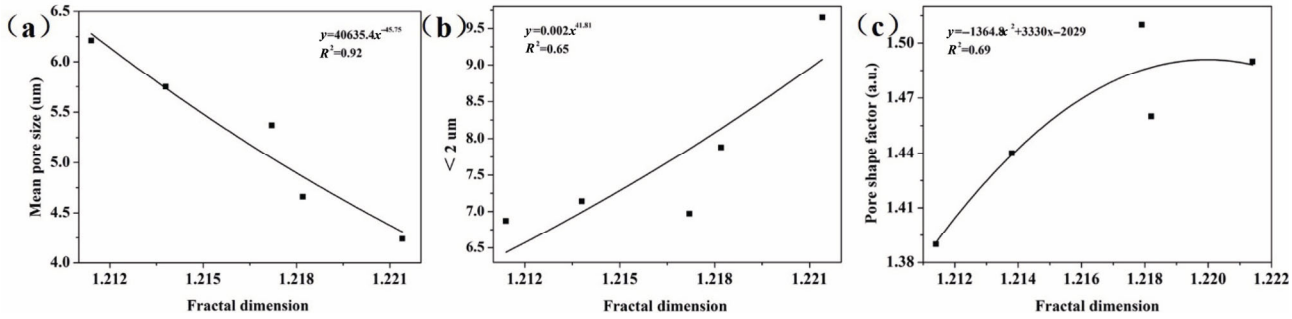

Fig. 9 Relationship between fractal dimension and pore structure: (a) mean pore size, (b) proportion of micro-pore < 2 μm, and (c) pore shape factor.

are negatively correlated with the MPS (Fig. 9(a)). D_f increases with increasing the proportion of < 2 μm micro-pores and pore shape factor (Figs. 9(b) and 9(c)), indicating that the proportion of < 2 μm pores and the pore shape factor are positively correlated with D_f. This result confirms that the reduction of MPS, improvement of both < 2 μm micro-pore proportion and pore shape factor lead to the increase of pore structure complexity. Based on the above analysis results, the correlation between thermal shock resistance and HMOR

as well as pore structure parameters can be characterized by the fractal dimension. It is possible to effectively enhance HMOR and thermal shock resistance by increasing MPS and pore sphericity of PAC, and especially the relatively irregular large pores and < 2 μm proportion of micro-pores should be avoided.

4 Conclusions

Porous alumina ceramics exhibiting various pore size and pore distribution by incorporating of different types of carbon black as pore-forming agent were successfully fabricated. Fractal dimension and regression analysis were applied to investigate the influence of pore size and its distribution, as well as their combined effect on material mechanical property and thermal property. The fractal dimension of pore structure decreases with the increase of mean pore size. From the viewpoint of fractal dimension and results obtained from regression analysis, the improvement of mechanical strength and thermal shock resistance parameters (R_{st}) of porous alumina ceramics can be obtained by increasing their mean pore size, pore sphericity and decreasing the proportion of < 2 μm micro-pores.

Excellent hot modulus of rupture (6.26 MPa) and thermal shock resistance parameter (R_{st} , 2.53) for specimen C37 are obtained, whose porosity is 65.9%. Fractal dimension can be also adopted to investigate other porous ceramic systems, and such novel method also exhibits the broad applicability to analyze ceramics with a wide range of porosity levels.

Acknowledgements

The authors are grateful for the financially support from the National Basic Research Program of China (973 Program, Grant No. 2012CB722702), the National Natural Science Foundation of China (Grant No. 51572140), the China Postdoctoral Science Foundation (Grant No. 2017M610085), and the China Postdoctoral Science Foundation (Grant No. 2016T90092).

References

[1] Gregorová E, Pabst W, Živcová Z, *et al*. Porous alumina ceramics prepared with wheat flour. *J Eur Ceram Soc* 2010, **30**: 2871–2880.

[2] Shimizu T, Matsuura K, Furue H, *et al*. Thermal conductivity of high porosity alumina refractory bricks made by a slurry gelation and foaming method. *J Eur Ceram Soc* 2013, **33**: 3429–3435.

[3] Han M, Yin X, Cheng L, *et al*. Effect of core–shell microspheres as pore-forming agent on the properties of porous alumina ceramics. *Mater Design* 2017, **113**: 384–390.

[4] Li DS, Lu ZQ, Zhao JZ. Development of alumina bubble brick with good shock resistance. *Naihuo Cailiao* 1997, **31**: 284–285. (in Chinese)

[5] Zang W, Guo F, Liu J, *et al*. Lightweight alumina based fibrous ceramics with different high temperature binder. *Ceram Int* 2016, **42**: 10310–10316.

[6] Zake-Tiluga I, Svinka V, Svinka R, *et al*. Thermal shock resistance of porous Al_2O_3–mullite ceramics. *Ceram Int* 2015, **41**: 11504–11509.

[7] Singh AK, Sarkar R. Development of spinel sol bonded high pure alumina castable composition. *Ceram Int* 2016, **42**: 17410–17419.

[8] Shyam A, Bruno G, Watkins TR, *et al*. The effect of porosity and microcracking on the thermosmechanical properties of cordierite. *J Eur Ceram Soc* 2015, **35**: 4557–4566.

[9] Jin X, Dong L, Xu H, *et al*. Effects of porosity and pore size on mechanical and thermal properties as well as thermal shock fracture resistance of porous ZrB_2–SiC ceramics. *Ceram Int* 2016, **42**: 9051–9057.

[10] She JH, Beppu Y, Yang JF, *et al*. Effects of porosity on thermal shock resistance of silicon nitride ceramics. In Proceedings of the 26th Annual Conference on Composites, Advanced Ceramics, Materials, and Structures: B: Ceramic Engineering and Science Proceedings, 2002, **23**: 247–252.

[11] Hasselman DPH, Ziegler G. On the effect of crack growth on the scatter of strength of brittle materials. *Ceram Int* 1985, **11**: 134.

[12] Li Y, Li X, Zhu B, *et al*. The relationship between the pore size distribution and the thermo-mechanical properties of high alumina refractory castables. *Int J Mater Res* 2016, **107**: 263–268.

[13] Lee WJ, Cho YJ, Lee HS, *et al*. Effect of pore morphology on elastic, heat conduction and thermal shock fracture behaviors of porous ceramics. *Procedia Engineering* 2011, **10**: 2459–2463.

[14] Jin X, Dong L, Xu H, *et al*. Effects of porosity and pore size on mechanical and thermal properties as well as thermal shock fracture resistance of porous ZrB_2–SiC ceramics. *Ceram Int* 2016, **42**: 9051–9057.

[15] Foroutan-Pour K, Dutilleul P, Smith DL. Advances in the implementation of the box-counting method of fractal dimension estimation. *Appl Math Comput* 1999, **105**: 195–210.

[16] Barbera PL, Rosso R. On the fractal dimension of stream networks. *Water Resour Res* 1989, **25**: 735–741.

[17] Wei G-P, Zhu B-Q, Li X-C, *et al*. Correlativity between pore structure parameters and thermal conductivity of

cenosphere insulating refractory. *Journal of Functional Materials* 2012, **43**: 3432–3436.
[18] Wang S, Deng C, Zhang X, *et al*. Pore volume fractal dimension of magnesium olivine heat insulation materials. *Journal of the Chinese Ceramic Society* 2015, **43**: 351–357.
[19] Pia G, Sanna U. An intermingled fractal units model and method to predict permeability in porous rock. *Int J Eng Sci* 2014, **75**: 31–39.
[20] Pia G, Casnedi L, Sanna U. Porous ceramic materials by pore-forming agent method: An intermingled fractal units analysis and procedure to predict thermal conductivity. *Ceram Int* 2015, **41**: 6350–6357.
[21] Zhu B, Wei G; Li X. Characteristization of pore size distribution for porous insulating refractories by image analysis technique. *Journal of the Chinese Ceramic Society* 2012, **40**: 1369–1375.
[22] Jin S, Zhang J, Han S. Fractal analysis of relation between strength and pore structure of hardened mortar. *Constr Build Mater* 2017, **135**: 1–7.
[23] Liu J, Li Y, Li Y, *et al*. Effects of pore structure on thermal conductivity and strength of alumina porous ceramics using carbon black as pore-forming agent. *Ceram Int* 2016, **42**: 8221–8228.
[24] Fu L, Gu H, Huang A, *et al*. Possible improvements of alumina–magnesia castable by lightweight microporous aggregates. *Ceram Int* 2015, **41**: 1263–1270.
[25] Veljović D, Jančić-Hajneman R, Balać I, *et al*. The effect of the shape and size of the pores on the mechanical properties of porous HAP-based bioceramics. *Ceram Int* 2011, **37**: 471–479.
[26] Zhong X, Zhao H. High-temperature properties of refractory composites. *Am Ceram Soc Bull* 1999, **78**: 98–101.
[27] Hasselman DPH. Unified theory of thermal shock fracture initiation and crack propagation in brittle ceramics. *J Am Ceram Soc* 1969, **52**: 600–604.
[28] Hasselman DPH. Elastic energy at fracture and surface energy as design criteria for thermal shock. *J Am Ceram Soc* 1963, **46**: 535–540.
[29] Kingery WD. Factors affecting thermal stress resistance of ceramic materials. *J Am Ceram Soc* 1955, **38**: 3–15.
[30] Thomas Jr. JR, Singh JP, Hasselman DPH. Analysis of thermal stress resistance of partially absorbing ceramic plate subjected to asymmetric radiation, I: Convective cooling at rear surface. *J Am Ceram Soc* 1981, **64**: 163–169.
[31] Kayama A, Tanaka M, Kato R. Application of slit island method to the evaluation of the fractal dimension of the grain-boundary fracture in high-temperature creep. *J Mater Sci Lett* 2000, **19**: 565–567.